

**Accessing the Low-polar Molecular Composition of Boreal and Arctic Peat Burning Organic  
Aerosol via Thermal Analysis and Ultrahigh-Resolution Mass Spectrometry: Structural Motifs  
and Their Formation**

Eric Schneider<sup>1,2</sup>, Anika Neumann<sup>1,2</sup>, Martha L. Chacón-Patiño<sup>3</sup>, Markus Somero<sup>4</sup>, Meri M. Ruppel<sup>5</sup>, Mika Ihalainen<sup>4</sup>, Kajar Köster<sup>4</sup>, Olli Sippula<sup>4,6</sup>, Hendryk Czech<sup>1,7</sup>, Christopher P. Rüger<sup>1,2,\*</sup>, Ralf Zimmermann<sup>1,2,7</sup>

<sup>1</sup>Joint Mass Spectrometry Centre, Department of Analytical and Technical Chemistry, University of Rostock, 18059 Rostock, Germany

<sup>2</sup>Department Life, Light & Matter (LL&M), University of Rostock, 18059 Rostock, Germany

<sup>3</sup>National High Magnetic Field Laboratory, Florida State University, 32310 Tallahassee, United States

<sup>4</sup>Department of Environmental and Biological Sciences, University of Eastern Finland, 70210 Kuopio, Finland

<sup>5</sup>Atmospheric Composition Unit, Finnish Meteorological Institute, 00014 Helsinki, Finland

<sup>6</sup>Department of Chemistry, University of Eastern Finland, 80101 Joensuu, Finland

<sup>7</sup>Joint Mass Spectrometry Centre, Cooperation Group “Comprehensive Molecular Analytics” (CMA), Helmholtz Centre Munich, 85764 Neuherberg, Germany

Corresponding author email: Christopher P. Rüger ([christopher.rueger@uni-rostock.de](mailto:christopher.rueger@uni-rostock.de))

**Keywords:**

peat burning, organic aerosol, ultrahigh-resolution mass spectrometry, thermal analysis, infrared multiphoton dissociation (IRMPD), structural motifs

## **Abstract**

Peatland fires emit organic carbon rich particulate matter into the atmosphere. Boreal and Arctic peatlands are becoming more vulnerable to wildfires, resulting in a need for better understanding of the emissions of these special fires. Extractable, non-, and low-polar organic aerosol species emitted from laboratory-based boreal and Arctic peat burning experiments are analyzed by direct-infusion atmospheric pressure photoionization (APPI) ultrahigh-resolution mass spectrometry (UHRMS) and compared to time-resolved APPI UHRMS evolved gas analysis from the thermal analysis of peat under inert nitrogen (pyrolysis) and oxidative atmosphere. The chemical composition is characterized on a molecular level, revealing abundant aromatic compounds that partially contain oxygen, nitrogen or sulfur and are formed at characteristic temperatures. Two main structural motifs are identified: single-core and multicore, and their temperature dependent formation is assigned to the thermal degradation of the lignocellulose building blocks and other parts of peat.

## 1. Introduction

Particulate matter (PM) emitted from biomass burning (BB) directly affects the radiation budget of the atmosphere and likewise constitutes a risk for human health.<sup>1-3</sup> In addition to those particles' physical properties (size, shape), the chemical properties, *e.g.*, oxidative potential, light absorption ability or acting as cloud condensation nuclei, are affected by the complex molecular composition of the organic carbon (OC) fraction. The characterization of the highly variable composition of the organic aerosol (OA) provides information on factors like fuel type, combustion conditions and the degree of atmospheric processing.

Peatland fires are known to emit particularly high amounts of OC rich PM and have been frequently observed in warmer climate regions such as southeast Asia and southern Africa.<sup>4,5</sup> However, globally, the largest deposits of peat are found in the northern hemisphere in boreal and Arctic peatlands, and the composition of PM emitted from these fires is not yet well characterized.<sup>6-8</sup> Climate change and the resulting increased temperatures as well as higher frequency of extreme weather events, like droughts and thunderstorms, increase the size and frequency of wildfires also in boreal and Arctic regions.<sup>9-11</sup> Peatland fires, often associated with forest fires, are expected to follow this trend.<sup>3,12</sup>

Boreal and Arctic peatlands are home to a large variety of vascular and non-vascular plants including especially various species of sedges, shrubs, and *Sphagnum* mosses. Peat layers are formed by the accumulation of incompletely decomposed plant material partially transformed into humic substances by biodegradation.<sup>13</sup> With increasing depth of the peat layer, the maturation of fresh biomass increases due to methanogenesis under anaerobic conditions, consequently forming fossilized materials by coalification.<sup>14</sup> Peatlands are typically affected by smoldering fires which are characterized by oxygen-deficient, slow, flameless burning and low temperatures (up to 600 °C) by heterogenous oxidation and a lower modified combustion efficiency (MCE; higher ratio of CO to CO<sub>2</sub>). In contrast, flaming combustion takes place at higher temperatures (1500 °C) and involves fuel volatilization by pyrolysis with subsequent homogeneous oxidation in the oxygen-rich gas phase with a higher MCE.<sup>15-17</sup>

For the chemical characterization of peat burning derived OA, PM can be collected on filter samples and extracted for in-depth offline analysis. Targeted approaches like gas chromatography coupled to mass spectrometry (GC-MS) are used to identify and quantify known marker compounds but miss a large proportion of the low-volatile OC fractions.<sup>18</sup> To address the high complexity of combustion aerosols, direct-infusion Fourier transform ion cyclotron resonance (FT-ICR) MS enables the characterization of a wide mass and volatility range. Its ultrahigh resolution and mass accuracy allows for the assignment of sum formulas of compounds comprised of C, H, N, O and S.<sup>19</sup> Moreover, selective ionization techniques, e.g., electrospray ionization (ESI) targeting polar compounds and atmospheric pressure photoionization (APPI) targeting non-/low-polar species can be utilized to address a specific compositional space.<sup>20</sup> With respect to the unique composition and burning conditions of boreal and Arctic peats compared to other wildfire fuel types, FT-ICR MS have shown an extreme molecular complexity including polar nitrogen- and sulfur-rich OA compounds that were found to be clearly different comparing boreal and Arctic peat.<sup>21–23</sup>

The origin of the complex composition of fresh peat-derived OA could be accessed by online chemical analysis of laboratory-scale peat smoldering elucidating formation processes of the found organic compounds. Thermo-gravimetric analysis (TGA) provides a valuable basis to mimic combustion conditions as measurement atmospheres (inert, oxidative) and temperature programs can be controlled. The evolved gas mixture emitted during TGA can be further analyzed to obtain insights into the chemical composition of evaporation, pyrolysis, or combustion processes. As an example, TGA revealed different temperature ranges for the decomposition of remaining lignocellulosic biomass in peat that could be attributed to cellulose, hemicellulose, and lignin.<sup>24</sup> Evolved gas analysis (EGA) by Fourier transform infrared spectroscopy (FTIR) and MS showed temperature-dependent differences in the evolution profiles of gases and small organic compounds, that were also referred to lignocellulosic biomass decomposition.<sup>25</sup> The application of UHRMS for evolved gas analysis revealed in-depth characterization of lignin pyrolysis products as well as insights into wildfire-related changes in soil organic matter (SOM).<sup>26,27</sup>

FT-ICR MS in combination with EGA, but also with fragmentation techniques, such as infrared multiphoton dissociation (IRMPD), allow for insights into structural motifs of macromolecules based on pyrolysis products,<sup>28</sup> or fragmentation patterns,<sup>29</sup> respectively. Two main structural motifs can be assigned: single-core (island) and multicore type (archipelago). The single-core motif is comprised of larger condensed aromatic ring structures with alkylation, whereas the multicore motif is characterized by smaller interconnected aromatic ring structures.<sup>30</sup> This concept was initially applied to asphaltenes in petroleum but later transferred to OA from brown coal and biomass burning.<sup>21,31</sup> For OA, single-core structures are built up during combustion from smaller aromatic structures or humic substances formed by microbial degradation of biomass during peat maturation.<sup>32,33</sup> Multicore motifs are derived from lignin structures, soil organic matter biodegradation products (humic substances) or their incomplete thermal degradation.

34

This study aims to access the complex molecular composition and structural motifs of low and non-polar species formed during boreal and Arctic peat burning. The molecular complexity of real-world peat combustion aerosol is addressed by direct infusion ultra-high resolution APPI-FT-ICR MS. Additional IRMPD fragmentation experiments were applied on selected precursor compounds to access information on prevalent core structures present in the aerosol. The analysis conception is broadened by EGA-FT-ICR MS mimicking peat burning under oxygen-rich and inert nitrogen conditions on a small-scale laboratory basis. Because of comparatively low temperatures and slow heating rates of the TGA, we could mimic especially smoldering-like conditions. Oxygen-rich conditions can mimic smoldering in the upper soil layers that contain higher oxygen concentrations, whereas inert nitrogen conditions mimic particularly smoldering or heat-induced reactions in deeper soil layers with limited access to oxygen. Both IRMPD and EGA experiments are able to elucidate structural molecular motifs and provide insights into the single- versus multicore discussion of peat and peat burning aerosol. The combination of this complementary analytical

information adds molecular knowledge on OC-rich PM emissions from peatland fires in the northern hemisphere, increasing the understanding of their diverse climate and environmental health effects.

## **2. Materials and Methods**

### **2.1. Peat sampling sites and laboratory burning experiments**

A detailed description of the peat sampling sites and the laboratory burning experimental set up was given in a previous publication.<sup>21</sup> Briefly, 30 cm deep peat samples (top layer) were collected at four locations in northern Europe. Two samples were collected from Finnish Boreal peatlands (Lakkasuo: FIA, Siikaneva: FIB) and two sample were collected from permafrost peatlands in Rogovaya (ROG; Russia) and on Svalbard (NOR; Norway) (Table 1). At the Finnish Boreal peatland sites, samples from deeper layers (30-60 cm) were collected additionally, for thermal analysis. All samples were stored under dark and dry conditions until the combustion experiment. Both Finnish peat samples (FIA, FIB) were collected from ombrotrophic boreal peatlands characterized by a vegetation dominated by Sphagnum moss cover as well as sedges, some small shrubs and birch trees. In contrast, the samples ROG and NOR originate from the active layer of Arctic permafrost peatlands that experience lower peat formation due to the harsher climatic conditions. The main vegetation at the minerotrophic ROG sampling site is dominated by sedges and, to a lesser extent, Sphagnum mosses and some shrubs. The vegetation at the Svalbard study site (NOR) is characterized as herbaceous moss tundra.

Open peat burning was conducted at the ILMARI-laboratory of the University of Eastern Finland.<sup>35</sup> 50 g of each top-layer peat sample was placed in the burning stove and ignited by a heating element within the sample. The formed exhaust gases were collected by a hood and transferred to connected on-line instrumentation and filter sampling. Particulate matter (PM) samples were collected from the exhaust aerosols on pre-baked quartz fiber filters (QFF, Pallflex Tissuquartz) for 12–55 min (depending on the duration of the combustion) with a flow rate of 90 l min<sup>-1</sup>. Fourier Transform Infrared Spectroscopy (FTIR,

DX4000, Gaset, Finland) was used to measure carbon monoxide and carbon dioxide was measured by an NDIR-based trace level CO<sub>2</sub> gas analyzer (ULTRAMAT 23, Siemens, Germany) to define the start and end point of the combustion experiment (above or below 5 ppm CO, respectively) and to calculate the modified combustion efficiency (MCE).<sup>17</sup>

## 2.2. Thermal Gravimetric Analysis and Time-resolved Ultrahigh-Resolution Mass Spectrometry

For thermal gravimetric analysis (TGA), aliquots of each peat were cryo-milled to create homogenized samples. Few milligrams (7–22 mg) of the powder were weighted in aluminum crucibles and placed in the thermobalance (TG 209, Netzsch Gerätebau, Selb, Germany) coupled to a modified Bruker GC-APCI II source equipped with atmospheric pressure photoionization (APPI) by a Kr vacuum ultraviolet lamp (10/10.6 eV, 124/117 nm) operated in positive ion mode.<sup>36,37</sup> The temperature gradient of the thermobalance was programmed to start with a 2 min isothermal step at 30 °C, then a ramp to 600 °C (10 K min<sup>-1</sup>), and a final isothermal step for 15 min at 600 °C, with a constant flow of 200 mL min<sup>-1</sup> compressed air or nitrogen, depending on the experiment (Table 1). The evolved mixture was sampled via a heated interface and transfer line (deactivated fused silica capillary, 0.53 mm inner diameter, 280 °C) into the ion source of the mass spectrometer. For mass spectrometric detection, a Fourier-transform ion cyclotron resonance mass spectrometer (FT-ICR MS; Apex II Ultra FT-MS, Bruker, Germany) was used, equipped with a 7 T superconducting magnet. Mass spectra were recorded in the range of  $m/z$  100–1000 with a four megaword transient, resulting in a resolving power of approx. 300,000 at  $m/z$  400. Time-resolved broadband spectra were recorded by accumulating 10 microscans that result in an acquisition rate of 3 summed spectra per minute. A detailed description of the combined setup can be found elsewhere.<sup>38</sup>

**Table 1:** Overview of peat samples (top layer: 0-30cm), conditions during thermal analysis and resulting mass loss after the temperature protocol and keeping the sample for 15 min at 600 °C.

| origin                 | classification | sample | atmosphere            | mass [mg]     | residue [%] | mass loss [%] |
|------------------------|----------------|--------|-----------------------|---------------|-------------|---------------|
| Lakkasuo<br>(Finland)  | boreal         | FIA    | nitrogen<br>oxidative | 7.37<br>6.77  | 23<br>2     | 77<br>98      |
| Siikaneva<br>(Finland) | boreal         | FIB    | nitrogen<br>oxidative | 8.21<br>10.05 | 25<br>2     | 75<br>98      |
| Svalbard<br>(Norway)   | Arctic         | NOR    | nitrogen<br>oxidative | 9.27<br>21.7  | 59<br>43    | 41<br>57      |
| Rogovaya<br>(Russia)   | Arctic         | ROG    | nitrogen<br>oxidative | 8.72<br>12.6  | 29<br>5     | 71<br>95      |

### 2.3. Filter Extraction and Direct-infusion Ultrahigh-Resolution Mass Spectrometry

Portions of each QFF sample were extracted in cleaned glass vials with 4 ml methanol/dichloromethane (1/1 v%, LC-MS grade) and ultra-sonication for 30 min in an ice chilled water bath. Finally, the extracts were filtered (0.22 µm PTFE membrane, Sartorius, Goettingen, Germany) to remove any remaining particles and stored at -25 °C until analysis. Prior to the analysis, an aliquot of 0.5 ml of each sample was diluted with 4 ml methanol/toluene (1/1 v%).

Direct-infusion broadband APPI FT-ICR MS measurements were performed at the National High Magnetic Field Laboratory in Tallahassee (Florida, USA) on a custom-built hybrid linear ion trap FT-ICR mass spectrometer equipped with a 21 T superconducting magnet.<sup>39</sup> Time domain transients of 3.2 s were conditionally co-added (100 scans) to achieve comparable total ion abundances.  $2 \times 10^6$  charges were externally accumulated and transferred to the ICR cell for analysis.

#### 2.4. Fragmentation: Infrared multiphoton dissociation

For infrared multiphoton dissociation (IRMPD) at the 21 T FT-ICR MS, ions of a 2 Da mass window ( $m/z$  559-561) were isolated by the external dual linear ion trap, accumulated and transferred to the ICR cell, fragmented by irradiation for 500 ms with an IR-laser ( $\lambda = 10.6 \mu\text{m}$ , 40 W, Synrad CO<sub>2</sub> laser, Mukilteo, USA) inside the ICR cell and consequently detected.<sup>29</sup> Time domain transients of 3.2 s were conditionally co-added (200 scans) to achieve comparable total ion abundances.

#### 2.5. Data Analysis and Sum Formula Assignment

Data analysis of direct-infusion 21 T FT-ICR MS data (broadband and fragmentation experiments) was carried out with Predator Analysis. It was used for the processing of coadded time-domain transients, including phasing (only broadband), Fourier-transformation, peak picking (peaks greater than six times the baseline root-mean-square noise at  $m/z$  400) and mass calibration, based on selected intensive Kendrick mass series covering the whole mass range and consequent walking calibration.

For time-resolved TGA 7 T FT-ICR MS, DataAnalysis 5.1 (Bruker, Germany) was used for peak picking (S/N of  $\geq 6$ ), internal calibration with intensive homologous series and export of the time-resolved data by a self-written Visual Basic script.

The exported mass spectra from both instruments were processed by self-written MatLab algorithms and routines combined in a graphical user interface named CERES Processing.<sup>40</sup> After careful manual investigation, the following restrictions were deployed for elemental composition assignment:  $\text{C}_c\text{H}_h\text{N}_n\text{O}_o\text{S}_s$ , where  $5 \leq c \leq 100$ ,  $5 \leq h \leq 100$ ,  $n \leq 4$ ,  $o \leq 15$ , and  $s \leq 2$ , with a maximal error of  $\pm 0.3$  ppm for direct-infusion data or  $\pm 1$  ppm for time-resolved data, allowing for the assignment of radical cations and protonated species ( $\text{M}^+ / [\text{M}+\text{H}]^+$ ).

FT-ICR mass spectra files and assigned elemental compositions are publicly available via the Open Science Framework at DOI 10.17605/OSF.IO/B8FDU.<sup>41</sup>

### 2.5.1 Double bond equivalents (DBE) and Planar Aromatic Limit

Double bond equivalents (DBE) are a measure for the degree of unsaturation. It is defined as the sum of the number of double bonds ( $\pi$ -bonds) and rings in a molecule and can be calculated based on the assigned elemental composition:  $DBE = C - H/2 - N/2 + 1$ . DBE versus carbon number plots are used to visualize complex datasets and emphasize changes in the degree of unsaturation in combination with the size (carbon number) of molecules. The planar limit, defined as the line generated by connecting the maximum DBE values of given carbon numbers based on the maximum valence of carbon, can be applied to assign structural building blocks of compounds.<sup>42</sup>

## 3. Results and Discussion

### 3.1. Extractable Low-polar Species in Boreal and Arctic Peat Burning PM

The laboratory-based burning of the two Boreal and two Arctic peat samples is dominated by smoldering combustion, indicated by low to medium MCE values during the burning phase (MCE = 0.82–0.92, Table S1), producing high amounts of OC-rich PM because of incomplete thermal peat degradation. PM extracts of those samples are characterized by (+)APPI 21 T FT-ICR MS analyses and reveal a complex mixture of non- and low-polar organic constituents (Figure 1a), mostly assigned to the CHO, CH, CHNO and sulfur-containing compound classes in the range of  $m/z$  180–600. The average DBE (8.63–9.43) and  $AI_{mod}$  (0.39–0.43) values are consistently high, indicating a strong abundance of molecules that contain aromatic ring structures (Figure 1b, Figure S3). However, in general, all four peat combustion extracts are vastly similar, both regarding the detected elemental compositions (70–87 % common compounds, Figure S1) as well as their intensity distribution in the mass spectra (Figure S2), even though APPI is reported to be less prone to matrix effects.<sup>20</sup> This result contrasts with observations made for the polar organic fraction of these aerosol extracts investigated in a previous study by ESI 21 T FT-ICR MS, that revealed distinct differences between the boreal and Arctic peat burning aerosols in all compound classes.<sup>21</sup> With regard to Figure 1,

the CHO class is the most abundant compound class (approx. 50-54% int.) with molecules containing up to 10 oxygen atoms, but predominantly with small oxygen numbers (average #O: 1.8–2.0), resulting in low intensity weighted average O/C ratios of 0.14–0.16, which is lower than would be expected for, *e.g.*, lignin (Table S2, Table S3).<sup>38</sup> The DBE versus carbon number plot (Figure 1b) shows broad coverage of the compositional space, indicating condensed aromatic structures, close to the planar aromatic limit,<sup>43</sup> as well as less aromatic structures with more alkylation. CHO compounds originate during combustion from the incomplete thermal degradation of the main plant building structures cellulose, hemicellulose and lignin, which are all found, partially degraded, in the peat before combustion and may undergo further oxidation during the combustion process.<sup>44–46</sup>

The second most abundant compound class in the organic aerosol (OA) of peat burning is the CH class, followed by the CHS class, with both also covering the whole detected mass range. The CH class is dominated by condensed aromatic compounds (Figure 1b) but also species with lower aromaticity and higher alkylation were detected. Hydrocarbons are a known product from combustion processes and are therefore also expected for the smoldering combustion of peat, *e.g.*, in the form of PAHs or alkanes, which were often particularly abundant in peat burning emissions.<sup>47,48</sup> The low temperature smoldering conditions are also the reason for the observation of more alkylated hydrocarbon and PAH species, that would not be formed by *e.g.*, high temperature flaming combustion.<sup>49</sup>

The CHS class shows abundant signals in the high DBE range (Figure 1b), indicating the formation of sulfur-containing condensed PAHs (*e.g.*, Benzothiophenes) during peat burning. A dimeric or trimeric pattern of the main intensity distribution is observed, with maxima at DBE = 6, 9 and 12 (CHS1) and DBE= 8 and 11 (CHS2). CHS compounds have been rarely detected in primary emissions from biomass burning, as the amount of sulfur is low in most types of fresh biomasses.<sup>50</sup> Peat seems to be an exception to this, as the number of detected CHS as well as CHOS compounds is high in all samples. The reason for the high abundance of sulfur-containing species in peat smoldering organic aerosol could be the ability of

*Sphagnum* mosses to efficiently fixate sulfur as well as the microbial activity during the formation of peat under oxygen-depleted conditions, especially from sulfur-reducing microorganisms. The organosulfur species are therefore likely already present in the partially matured peat before being volatilized during combustion. Additionally, the ionization by APPI is very sensitive for sulfur-containing species, which may result in an overrepresentation of these species.<sup>51</sup> The herein discussed results are in line with our previous study, that revealed an unusually high abundance of sulfur-containing species (CHOS, CHNOS) in the polar fraction of the same peat combustion emission extracts.<sup>21</sup>

Nitrogen-containing species are found to be oxidized (CHNO) or reduced species (CHN) with high aromaticity in all samples, but with higher relative intensity in the two Arctic peat samples. Smoldering combustion is known to emit nitrogen-containing compounds from the low-temperature, oxygen-depleted combustion of biomass, and especially peat was found to emit high concentrations of e.g., pyridine-like compounds, which would fit the observed distribution in the DBE versus carbon number plot (Figure 1b).<sup>52</sup> The overall number and intensity of nitrogen-containing compounds is low compared to the other classes, which may partially be explained by their lower ionization efficiency in APPI.<sup>53,54</sup>

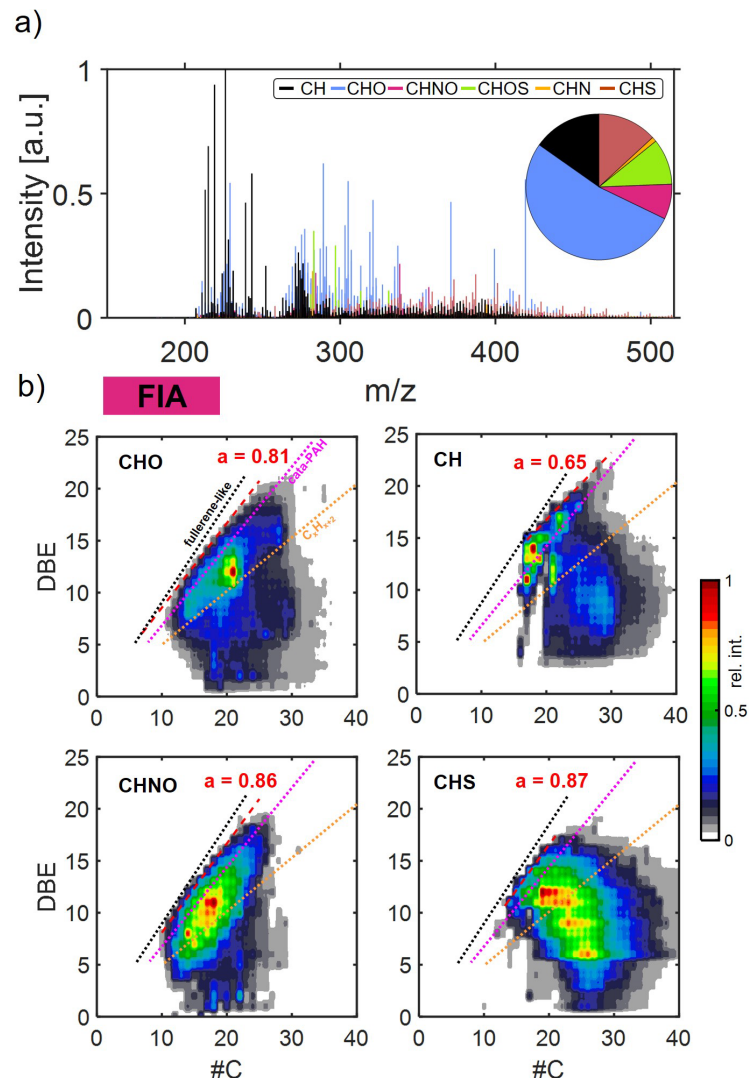


**Figure 1:** **a)** Mass spectrum of assigned elemental compositions for an exemplary peat PM extract sample (FIA) measured by direct-infusion 21T APPI FT-ICR MS. The compound class of each formula is indicated by its color and the relative intensity compound class distribution is indicated by the inserted pie chart. **b)** Contour plots of double bond equivalents (DBE) versus carbon number summarized into four major compound classes (CH, CHO<sub>x</sub>, CHN<sub>y</sub>O<sub>x</sub> and CHS<sub>z</sub>) for the exemplary peat PM extract sample FIA measured by 21 T APPI FT-ICR MS. Reference lines for fullerene-like hydrocarbons (black, DBE= 0.9 x C), cata-condensed PAHs (pink, DBE= 0.75 x C -0.5) and linear polyenes (orange, C<sub>x</sub>H<sub>x+2</sub>) are indicated by dotted lines. The planar limit of each compound class is calculated by a linear regression and the slope *a* is indicated by a red dotted line.

Although the non- and low-polar OA fractions of boreal and Arctic peat reveal high similarity with respect to compound occurrence and abundance pattern, they are still of relevance regarding the differentiation to other emission sources due to the observed nitrogen- and sulfur-containing compounds. While the polar organic fraction was found to contain highly oxygenated CHO, CHNO, CHOS and CHNOS species,<sup>21</sup> the low polar fraction analyzed in this study contains most of these compound classes, but more uniformly regarding the different peat samples, as well as less oxygen and higher abundances of the reduced compound classes CH, CHN and CHS. However, there are some differences between peat samples, observed in the low intensity region of the mass spectra, showing variances between the two origin regions of the peat samples (Boreal/Arctic). A number of common compounds from all compound classes is observed for the two Boreal peat samples (FIA + FIB: 1407) as well as several non- or low oxygenated nitrogen-containing compounds for the two Arctic peat samples (NOR + ROG: 416, unique NOR: 304, unique ROG: 523) (Figure S1). The origin of peat is therefore still a relevant factor that influences the chemical composition of the emitted organic aerosol, also regarding the low polar fraction of OC.

All detected compound classes show their center of intensity in the DBE versus carbon number plots close to the planar limit, with some also further extending to higher carbon numbers and lower DBEs. While compounds close to the planar limit can commonly be described as single-core compounds (island-type: large, condensed ring with low alkylation), compounds with lower DBE values and higher carbon numbers can be described as multicore compounds (archipelago-type: smaller aromatic rings connected by alkyl-bridges).<sup>28,30</sup> Both structural motifs are observed in all samples, with higher intensity of the single-core motif in most compound classes (Figure 1b, Figure S3).

### 3.1.1. Isolation and Fragmentation: IRMPD

Broadband mass spectrometric information gives limited access to structural information. However, the molecular structure determines the environmental, climate and health properties of the OA. For a deeper analysis of structural motifs in peat smoldering aerosol, extending beyond the interpretation of regions in the broadband DBE versus carbon number plots, isolation, and fragmentation of selected precursor masses by IRMPD is conducted (Figure 2a). The high chemical complexity does not allow for the external isolation of single compounds from direct-infusion experiments, but the isolation of 2 Da mass windows is feasible. The selected precursor mass range ( $m/z$  559–561) is on the upper end of the observed mass range, but extended ion accumulation times enable the accumulation of a sufficient number of ions for fragmentation. The fragment spectrum, therefore, represents a combination of fragments from an average of multiple hundred precursor ions and their corresponding molecular structures. This method has already been applied for the fragmentation and characterization of extremely complex petroleum samples.<sup>55</sup> The energy transfer in IRMPD occurs through the absorption of infrared radiation, exciting molecules into more energetic vibrational states, similar to a heating process causing thermal degradation.

56

The precursor region comprising the intact molecular ions is mainly comprised of CHO, CHNO as well as some CHN and CH compounds, representatively mimicking the overall class composition described above (Figure S4). However, the resulting fragment spectrum shows an entirely different compound class distribution, with high abundances of CH and CHN species in the lower mass range ( $m/z$  150–250). The corresponding DBE versus carbon number plots (Figure 2b) of the fragment ions separated by compound class reveals a narrow main region that is elliptically shaped and extends from DBE=4 (one ring) along the planar aromatic limit to DBE=30 (five rings or larger).<sup>57</sup> Compounds in this region can be described as condensed aromatic structures with a low degree of alkylation. These fragment species originate from archipelago-type precursor structures and are formed by the cleavage of bonds connecting the individual

condensed aromatic rings (2–6 membered rings), resulting in a diagonal shift from the precursor region to the bottom left of the DBE plots. The observation of condensed aromatic CHO, CHN, and CHNO compounds in the fragment spectrum indicates that the location of the heteroelements in these compounds is either inside the ring system or directly attached to the ring system, but not at the sidechains. In addition to the described main distribution, compounds with lower intensity are detected at high carbon numbers ( $\#C > 35$ ) in the CHO, CHN, and CHNO classes, shifted horizontally from the precursor region. These compounds are fragments from the dealkylation of single-core (island) precursor ions, as they only decrease in carbon number but not DBE, leaving the ring structure intact. Only a few of these species are observed, indicating a minor contribution of single-core motif compounds. Fragmentation by IRMPD, therefore, mainly cleaves condensed aromatic fragments from the precursor molecules, allowing the characterization of the core structures that form the precursor molecules.

In the APPI broadband spectrum, the single-core motif region shows the highest intensity, and it was also dominating in most of the spectra analyzed by ESI 21 T FT-ICR MS in a previous study,<sup>21</sup> but only a minor contribution of the expected dealkylation products is observed by IRMPD at  $m/z$  558–561. This observation could be explained by the selected mass region, which is at the upper end of the detected mass range and may, therefore, not address single-core species that are more frequently observed in the lower mass range. We hypothesize on different structural motifs along the molecular weight distribution of the peat OA, because of the incomplete thermal degradation of peat constituents. It is possible that the observed aromatic core structures are formed more efficiently through fragmentation by IRMPD.<sup>30,55</sup>

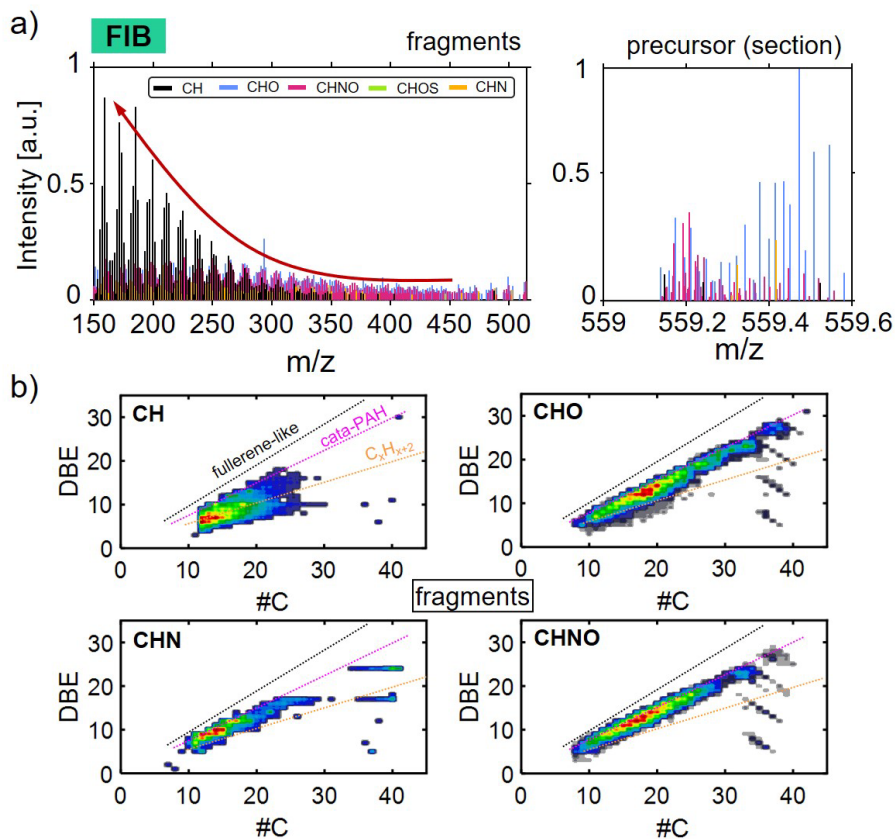


**Figure 2: a)** Mass spectra of assigned fragments (left) and zoom in on a section of precursor ions (right) in PM-extracts from the exemplarily combustion of peat FIB by infrared multiphoton dissociation (IRMPD) of an isolated precursor mass range ( $m/z$  559–561) by APPI 21T FT-ICR MS. The compound class of each peak is indicated by its color. The red arrow indicates the typical pattern of multicore precursor fragmentation.

**b)** Contour double bond equivalent (DBE) versus carbon number plots of the compound classes detected by IRMPD fragmentation of FIB. Reference lines for fullerene-like hydrocarbons (black,  $\text{DBE} = 0.9 \times \text{C}$ ), cata-condensed PAHs (pink,  $\text{DBE} = 0.75 \times \text{C} - 0.5$ ) and linear polyenes (orange,  $\text{C}_x\text{H}_{x+2}$ ) are indicated by dotted lines.

### 3.2. Thermal analysis APPI-FT-ICR MS of Boreal and Arctic peat

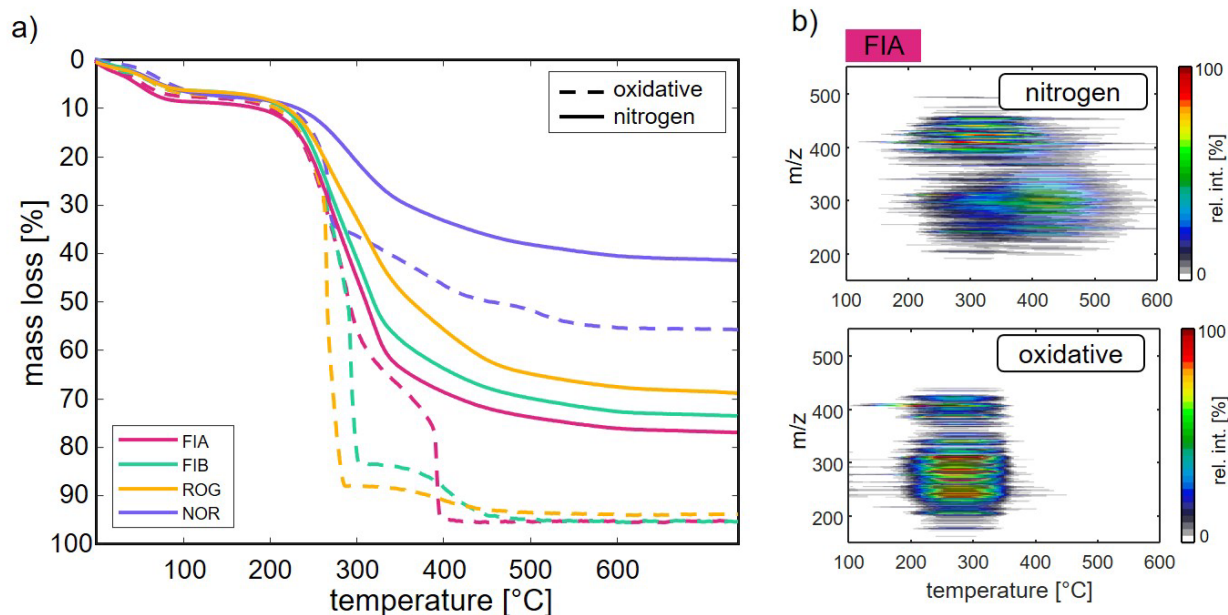
The origin and formation of organic aerosol compounds emitted from peat combustion can be further investigated by miniature-scale laboratory-based evolved gas analysis FT-ICR MS. Smoldering combustion conditions were aimed to be mimicked by TGA using inert nitrogen and oxidative atmosphere. The typical temperature of smoldering fires in peat ranges between 250–350 °C with peak temperatures of 600 °C, whereas flaming combustion occurs at peak temperatures of 1500 °C.<sup>58</sup> With the applied TGA setup, especially smoldering conditions can be simulated as the burning temperatures and propagation rates are comparatively low. Flaming combustion occurs at temperatures beyond the possibilities of our instrumentation. Therefore, the herein applied oxidative conditions more reflect smoldering fires in the upper peat layer in which oxygen concentration is still high, whereas inert nitrogen conditions can give insights into thermally induced reactions under poor oxygen conditions in deeper soil layers.

Figure 3a) shows the mass loss for all four peat samples under nitrogen and oxidative conditions with additional information on the exact mass loss values and residue content given in Table 1. Generally, oxidative conditions reveal higher mass losses than smoldering conditions that can be explained by more efficient combustion of the peat, whereas during oxygen-depleted smoldering, thermally induced condensation and aromatization reactions lead to the formation of coke residue.<sup>32,59</sup> NOR has in general higher TGA residues because of its higher mineral content. The sampling location of NOR is in the high arctic areas covered by ice or tundra with short vegetation.<sup>60</sup> Short and inefficient growing seasons lead to comparatively low peat formation that is why deposition of mineral soil has higher impact on the peat composition of NOR than for the other samples.

Regardless of the applied measurement atmosphere, all peat samples reveal a similar mass loss step between 30 to 100 °C that can be attributed to the evaporation of residual water.<sup>25</sup> At an onset temperature of approximately 200–250 °C, thermal decomposition and combustion of the organic material starts. Under oxidative conditions, combustion leads to an abrupt mass loss with a sharp DTG

signal (Figure S5). The main mass loss occurs below 300 °C, where most organic peat components undergo combustion.<sup>24</sup> However, there is a second mass loss step at 400 °C especially pronounced for FIA, but also present for the other peat samples. This second mass loss step might be attributed to peat compounds with a more stable carbon skeleton requiring higher temperatures for combustion. Those species might be humic substances, a broad group of larger soil organic compounds formed by microbial degradation of lignocellulosic biomass, which is characterized by functionalized, bridged and also higher aromatic molecular structures.<sup>13,61 33,62</sup> Therefore, we assume that the second mass loss step observed under oxidative combustion conditions could result from the combustion of larger aromatic structures of humic substances with higher humification degree. The idea of increased microbial matured compounds is further supported by the TGA data of the same peat sampled in greater depth as shown in Figure S6 (Table S5). Especially FIB sampled at 30–60 cm shows a pronounced second pyrolysis step at 400 °C compared to the less matured FIB sampled at 0–30 cm peat depth. Literature results also contribute to this hypothesis: humic substances extracted from forest-tundra peat reveal an increased aromatic content and, therefore, humification degree, with increasing depth of the peat layer.<sup>34</sup>

Under inert nitrogen conditions, the mass loss occurs over a broad temperature range of 200–500 °C and different pyrolysis features are highlighted in the DTG signal (Figure S5). Despite the water loss, there are three additional mass loss steps with maximum mass changes at 270 °C and 320 °C as well as a broader mass loss step between 380 °C to 500 °C. Peat is composed of partially degraded lignocellulosic biomass as well as its degradation products.<sup>63</sup> As we investigated the upper peat layer (0–30 cm) and consider the unfavorable degradation conditions especially in permafrost soil, these mass loss steps might be mainly attributed to hemicellulose, cellulose, and lignin. In literature, pyrolysis was observed for hemicellulose at 220–315 °C, for cellulose at 315–400 °C, and for lignin at a wider temperature range between 160 to 900 °C with most of the mass loss occurring at higher temperatures (400–550 °C).<sup>25,64</sup> Our TGA results on peat decomposition with inert and oxidative atmosphere especially fit these of Chen et al. studying Chinese forest peat.<sup>24</sup>



**Figure 3:** **a)** Mass loss curves of the four peat samples (FIA: magenta, FIB: green, ROG: yellow and NOR: blue) acquired by thermal analysis with oxidative (dashed line) or nitrogen (filled line) atmosphere. **b)** Temperature-resolved mass spectra of thermal analysis coupled to APPI FT-ICR MS of peat sample FIA measured under nitrogen (top) or oxidative (bottom) atmosphere.

Online-evolved gas analysis by high-resolution mass spectrometry provides additional information on the temperature-resolved chemical fingerprint of the different peat samples. In Figure 3b) and Figure S7, temperature-resolved mass spectra are shown for oxygen-depleted and oxygen-rich smoldering conditions. Summed mass spectra over the whole temperature range are given in Figure S8. In agreement with the before discussed TGA results, volatilized compounds are detected over a broad temperature range from 200–500 °C for inert nitrogen atmosphere, whereas for oxidative conditions, the temperature range is narrower (200–350 °C). In accordance with literature on biomass pyrolysis,<sup>38,64,65</sup> inert nitrogen conditions reveal a pronounced bimodal  $m/z$  distribution: The first  $m/z$  distribution is found for  $m/z$  380–500 with an intensity maximum between 200 to 350 °C, that might correspond to the pyrolysis of

hemicellulose and cellulose. The second  $m/z$  distribution is located at  $m/z$  200–350, with an intensity maximum between 400 to 550 °C, but starting, however, already at 200 °C. This second distribution is potentially produced by the pyrolysis of the lignin macrostructure cracked into smaller, oxygenated aromatics.

In Figure 4 and Figure S8, relative compound class distributions are given for the peat samples investigated under smoldering and oxidative conditions (intensity values normalized to the sample weight in Table S4). The samples FIA and ROG serve as examples for boreal and arctic peat, respectively. Absolute compound class distribution is shown in Figure S9. In general, the herein investigated peat from boreal regions reveals higher contents in oxygen-containing compounds, whereas the arctic peat is enriched in CH-class and nitrogen-containing compounds (N-, NO-class). These findings are in congruence with observations made for the laboratory-based peat combustion aerosol discussed above and ESI-FT-ICR MS results from a previous study.<sup>21</sup> Comparing both combustion conditions, oxygen-depleted smoldering releases an increased number of nitrogen-containing compounds. This effect is literature-known, and the presence of amides, nitriles, and N-heterocycles is related to reactions with increased concentration of ammonia during smoldering as well as the pyrolysis of biopolymers.<sup>66,67</sup> For peat smoldering, especially the release of pyridines was observed.<sup>52</sup>

It must be noted that EGA-FT-ICR MS did not detect any sulfur-containing compounds, although these compound classes sum up to one quarter of the relative intensity of the aerosol extracts discussed above. An explanation of this discrepancy might be the extraction process itself and, therefore, the enrichment of non- to semipolar compounds or the application of a dopant for the direct infusion analysis as well as the higher sensitivity, mass resolution and charge capacity of the 21 T FT-ICR MS system.

DBE/#C diagrams (Figure 4, Figure S10 & S11) add deeper insights on the molecular fingerprint of peat combustion products. Both combustion conditions reveal a bimodal DBE/#C distribution that is more pronounced for inert nitrogen conditions. The CH-class shows, regardless of the peat origin and for both

combustion conditions, an intensity maximum at 27–31 carbons and DBE values between 6–10. In literature, a variety of different organic compounds were identified in peat that includes n-alkanes, fatty acids, alcohols, squalene, but also cyclic compounds such as di- and triterpenoids or steroids.<sup>68,69</sup> However, the here observed DBE/#C range fit especially squalene (C<sub>30</sub>H<sub>50</sub>, DBE 6) and its derivatives or sterane-based biomarkers, which can also be ionized by APPI.<sup>54</sup>

The oxygen-containing classes reveal the most remarkable bimodal distribution in the DBE/#C diagram with a first distribution at 10–20 carbons and a second distribution at 25–30 carbons. In contrast to oxidative conditions, the occurrence of both distributions is related to temperature for inert nitrogen conditions. In Figure S12, evolution profiles of the oxygen-containing classes are shown for both combustion conditions. The O1–O4-classes reveal a first intensity maximum at temperatures between 200–350 °C and a second at 350–500 °C. At the first maximum, compounds with 27–31 carbons and DBE values between 4–10 were detected, that is in the same range as found for CH-class compounds. Although the temperature range of the first maximum is those of the decomposition of hemicellulose and cellulose, the detected sum formulae do not fit their expected pyrolysis products. Therefore, we assume that these detected compounds correspond to terpenoids, steroids or other cyclic organic species released during cellulose/hemicellulose pyrolysis. Similar can be assumed for higher oxygen classes occurring in that temperature range. At the second intensity maximum of the bimodal distribution, mainly O1–O4-class compounds with 10–25 carbons and DBE values between 4–15 were detected. These compounds are most likely oxygenated aromatics with low alkylation partially produced during the thermal decomposition of the lignin macrostructure. However, there is indication that also other macromolecular structures, like humic substances, contribute to this decomposition phase. The oxygen-containing pyrolysis products reveal a continuous compositional space without distinct evidence for the formation of dimers or trimers as it would be expected from the lignin macrostructure. It is therefore believed that also pyrolysis products of humic substances contribute to this phase.

As mentioned before, under inert nitrogen atmosphere, an increased number of nitrogen-containing species is detected compared to oxidative conditions. Both arctic and boreal peat reveal NO-compounds with 5–15 DBEs and relatively low carbon numbers of 10 to 20. The detected nitrogen-containing compounds seem to be mostly aromatic with relatively low alkylation. This finding indicates that nitrogen is mainly incorporated in aromatic rings rather than attached to alkyl side chains. Interestingly, also the nitrogen-containing compounds reveal a temperature dependence under inert nitrogen conditions (Figure S13).  $N_1O_x$ -compounds show a bimodal behavior with a first intensity maximum between 200–300 °C that could result from the thermal decomposition of more labile compounds. The second intensity maximum appears between 400 and 500 °C and could be attributed to the pyrolysis of N-containing macromolecules. Remarkably, nitrogen-containing compounds with two to three nitrogen atoms mostly occur at temperatures between 300–400 °C, that also suggests the decomposition of macromolecular structures. The comparison of the evolved gas emissions from both boreal and arctic peat indicates that the molecular composition of peat originating from different climatic regions has influence on the emitted compounds and, thus, also on the composition of real-world wildfire aerosols. The main differences are observed for oxygen- and nitrogen-containing compounds. Nitrogen-containing compounds are in general enriched in arctic peats (ROG, NOR); however, the structural motifs of emitted pyrolysis products are similar between both peat types. This is different for oxygen-containing compounds: the two investigated boreal peats (FIA, FIB) are clearly enriched in little alkylated, aromatic pyrolysis products that may originate from an increased content of lignin and/or humic substances in the peat organic matter. An increased content of lignin could be explained by the vegetation found at the boreal sampling sites compared to the arctic samples. The boreal peat sampling sites FIA/FIB were dominated by *sphagnum* mosses, sedges, some dwarf shrubs and birch trees, whereas the arctic sampling site ROG is characterized by dominating sedges and, to a lesser extent, *sphagnum* mosses and dwarf shrubs.<sup>21</sup> As the boreal peatlands are enriched in dwarf shrubs and birch trees, those plants seem to increase the lignin content in peat. Furthermore, an increased content of humic substances in boreal peat could be explained by a higher level of humification

caused by a higher microbial activity compared to permafrost arctic peat. Therefore, it is likely that a combination of both factors leads to the increased detection of small single-core pyrolysis products. However, as peat is a highly variable matrix, further investigations are needed to verify these assumptions. With respect to real world peat fire emissions, small-scale laboratory-based peat combustion with TGA-FT-ICR MS can add insights into thermally induced reactions. Our results nicely fit the observations of Solihat et al.,<sup>70</sup> who investigated the influence of peat burning on soil organic matter. The authors found an increase in compounds of smaller O-classes, the CH-class, and N-classes which is also indicated by our data. Furthermore, the authors investigated the onset temperature for the formation of smaller oxygen-containing compounds, that was determined to be between 300–400 °C. Also, this finding agrees with the results found for peat burning by TGA-FT-ICR MS, as we found the presence of lignin- or humic-like pyrolysis products in this temperature range typical for smoldering fires.

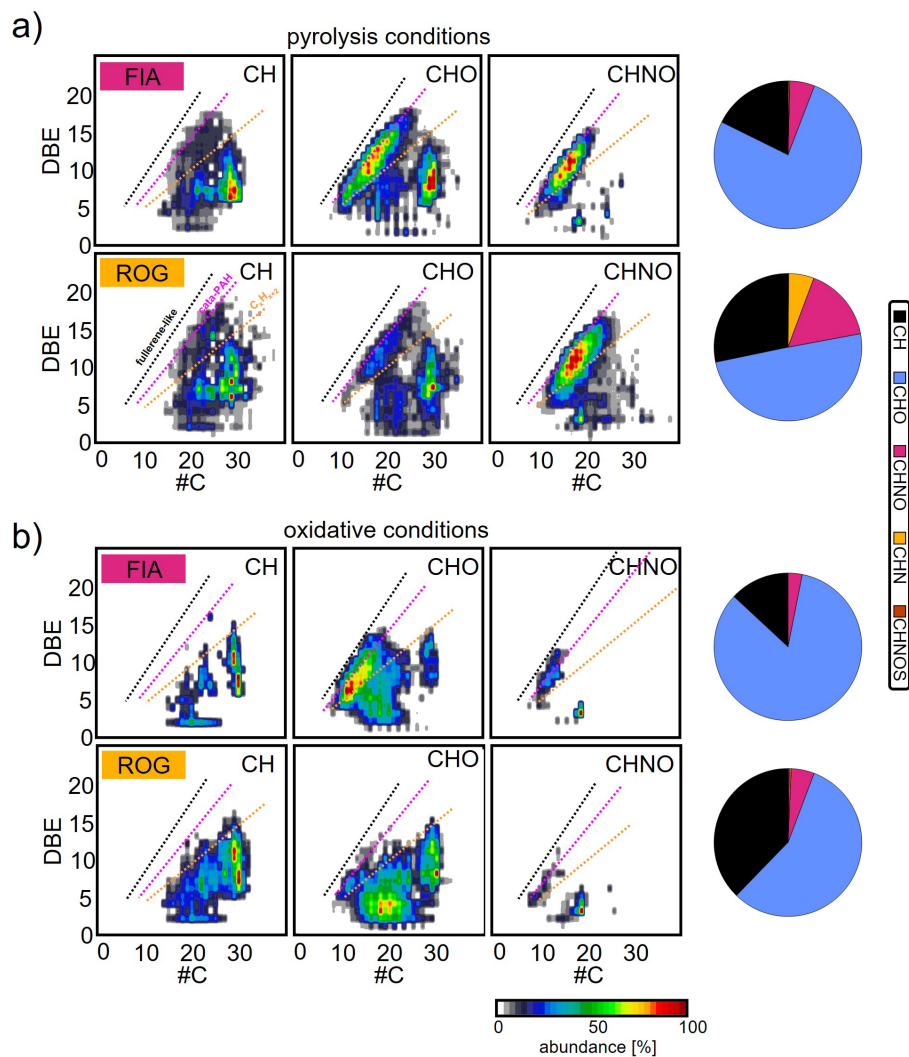


**Figure 4:** Contour plots of double bond equivalents (DBE) versus carbon number (#C) measured by TGA-FT-ICR MS for an example of boreal peat (FIA) and arctic peat (ROG). The contour plots are summed up over the whole temperature range (50-600 °C) and grouped into the three major compound classes (CH, CHO<sub>x</sub>, CHN<sub>y</sub>O<sub>x</sub>). All peat samples were investigated und a) inert nitrogen atmosphere and b) oxidative atmosphere. The relative compound class distribution for each sample is given as pie chart. Reference lines for fullerene-like hydrocarbons (black, DBE= 0.9 x C), cata-condensed PAHs (pink, DBE= 0.75 x C -0.5) and linear polyenes (orange, C<sub>x</sub>H<sub>x+2</sub>) are indicated by dotted lines.

### 3.3. Comparison of laboratory-scale peat burning and TGA experiments regarding chemical composition and structural motifs.

Laboratory-scale peat burning aerosol PM extracts reveal a significantly higher total number of detected compounds compared to the TGA experiments of the corresponding peat samples (Figure 5). This effect is to some extent caused by the higher dynamic range, ion capacity and scan accumulation of the direct infusion 21 T FT-ICR MS measurements used for the PM extract investigation and that leads to an increased detection of low intensity compounds. However, considering not only the number of common elemental compositions but also their intensity, 20–39% respectively 13–29% of the PM extract signal intensity can be assigned to compounds that are likewise detected in the TGA experiments under nitrogen or oxidative atmosphere of the same peat sample (Figure 5a).

Concerning only the number of detected elemental compositions, PM extracts and TGA under nitrogen atmosphere share the highest overlap, whereas the overlap with TGA under oxidative atmosphere is the lowest for all samples. With regard to the chemical composition, compounds common for all datasets are comprised of the CH and CHO class. Compounds uniquely shared by TGA with oxidative atmosphere and PM extracts are solely of the CHO class (Figure S14). In contrast, compounds shared by TGA under nitrogen atmosphere and PM extracts are comprised of CH, CHO, CHNO and CHN species, which fits, concerning also the higher number and intensity of the shared compounds, to the predominant smoldering combustion conditions.<sup>52,66</sup> Sulfur-containing classes were solely detected for PM extracts and were not found in the TGA experiments.

Although the number of compounds assigned to a specific emission scenario is low compared to the overall number of detected compounds in the PM extract, they represent a substantial fraction of the signal intensity and are therefore also likely emitted in relevant concentrations during real peat fire events. However, a large portion of signals found in the PM extracts is missed by the TGA mimicking, which shows

that TGA may explain only a limited fraction but does not fully reassemble the real-world combustion conditions, as these processes are much more complex.

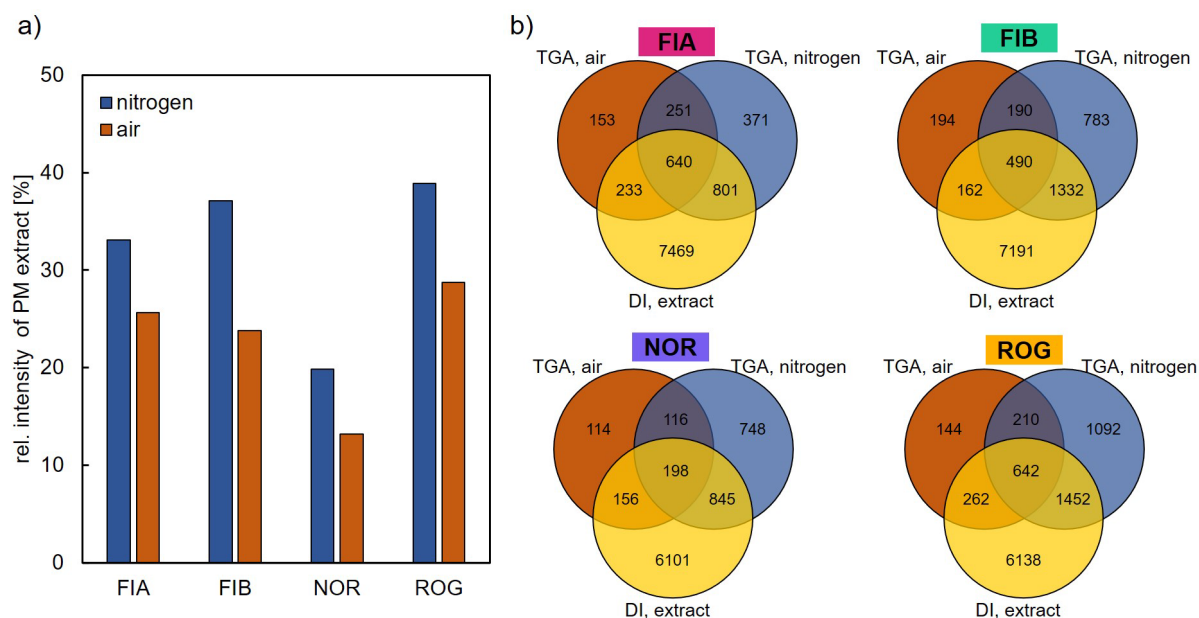


**Figure 5:** **a)** Relative intensity of compounds that are detected both during thermal analysis (TGA) with a nitrogen (blue) or oxidative (orange) atmosphere and the corresponding PM extract dataset. **b)** Venn diagrams of the intersect of elemental compositions detected by TGA with oxidative atmosphere, nitrogen atmosphere or by direct infusion (DI, yellow) of the combustion PM extracts.

Besides comparing the chemical composition of the peat burning aerosol PM extracts and the evolved gas analysis during the TGA of peat under oxygen/nitrogen atmosphere, also the molecular structural motifs of the emitted compounds were investigated in this study. The two main structural motifs (single-core and multicore) are observed for compounds from all three experiments, however, with different intensity. In Figure 6a, DBE/#C contour plots overlaid for all compound classes are shown with the single-core region marked in red and the multicore region marked in black. Especially TGA experiments under pyrolysis (nitrogen) conditions reveal two distinct regions in the DBE/#C diagram that match the expected regions

of both molecular structure types. This trend is less apparent in the data from TGA under oxidative atmosphere indicating a more extensive breakdown of the biomass during oxygen-rich combustion. The direct infusion data of the PM extracts reveal a highly pronounced single-core region, which might be explained by ionization effects of APPI. In literature, it was shown for asphaltenes, that APPI via direct-infusion may favor the ionization of single-core-type compounds in comparison to APPI via a gaseous sample inlet.<sup>28,55</sup>

Despite intensity differences in the structural motif regions, a similar trend for the oxygen classes O<sub>0</sub> to O<sub>8</sub> is observed in the single-core region for all datasets (Figure 6b). With the increasing number of oxygen atoms in a molecule, the relative portion of compounds observed in the single-core region increases from below 10% up to 100% (for TGA data). The same trend is also observed for the direct-infusion data of the PM extracts, but to a lower extent due to a higher number of compounds outside the single-core or multicore region. The boundaries for the population of the structural motifs are given in Table S6 and are based on the observed distribution in the TGA-FT-ICR MS data. It should be mentioned that this is a theoretical and simplified approach, as the natural distribution is a fluent transition of the two motifs. Furthermore, the concept was primarily considered for asphaltene research,<sup>30</sup> but is far from understood for other fields. Peat combustion emissions show a less distinct difference of the so-called island (single-core) and archipelago (multicore) motifs, that are observed in the petroleum derived asphaltenes, especially in data derived from the TGA-FT-ICR MS measurements.

Nonetheless, the structural dependence on the number of oxygen atoms allows for an indication of the formation processes of the respective compounds. Non to low oxygenated compounds (O<4) seem to be continuously formed up to high temperatures of 600 °C as suggested by TGA under pyrolysis conditions (Figure S12), whereas higher oxygen classes are formed at lower temperatures. This effect was also previously reported for other types of biomasses.<sup>37,38</sup> The unique composition of peat, containing partially degraded cellulose, hemicellulose, and lignin, may contribute to this stepwise formation behavior. At

lower temperatures, mainly cellulose and hemicellulose structures are thermally degraded, emitting compounds with more oxygen atoms and low alkylation. In contrast, lignin and humic-like structures are mainly degraded at higher temperatures (>420 °C), resulting in the emission of less oxygenated species.

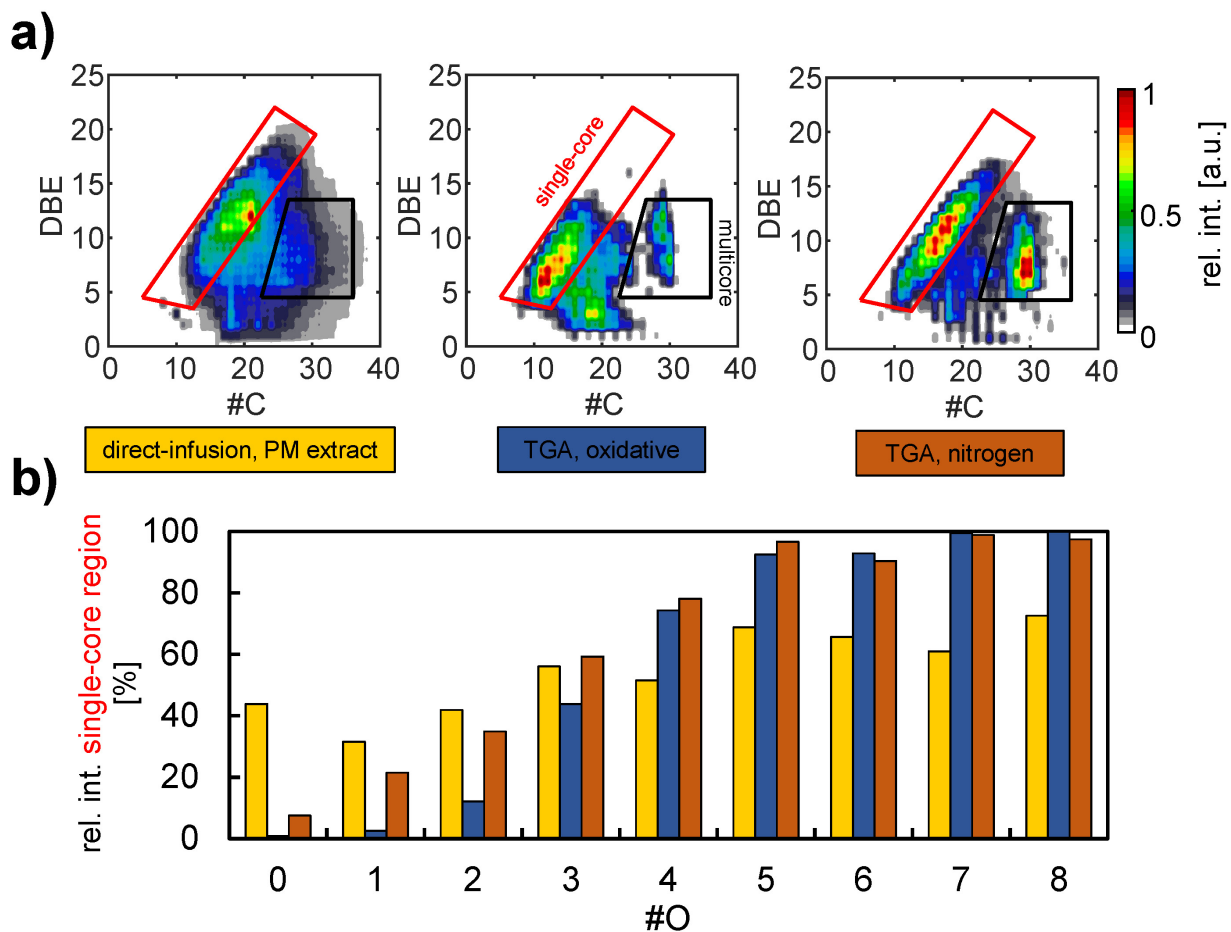


**Figure 6: a)** Double bond equivalent (DBE) versus carbon number (#C) contour plots of all elemental compositions detected by APPI FT-ICR MS for the peat sample FIA from direct-infusion of the PM extract (yellow) and thermal analysis (average over the whole temperature range) with nitrogen (blue) or air (orange) atmosphere. The DBE/#C region for the single-core structural motif is highlighted in red, whereas the multicore region is marked in black. **b)** Relative intensity of compounds detected inside the single-core region in dependence of the number of oxygen atoms.

#### 4. Conclusion

Non- and low-polar organic aerosol species emitted from boreal and Arctic peat burning were analyzed by combining laboratory-scale combustion experiments with miniature-scale simulation of the combustion process. Organic aerosol extracts and evolved gas emissions were characterized on the molecular level using state-of-the-art 21 T FT-ICR MS and TGA coupled to 7 T FT-ICR MS, respectively.

The organic aerosol extracts are vastly similar for all studied peat samples and are comprised of a complex mixture of partially oxygenated, highly aromatic compounds. The additional detection of nitrogen- and sulfur-containing compounds is a result of the predominant smoldering combustion of peat in combination with the unique formation process and composition of peat. Based on the assigned elemental compositions and calculated molecular properties, two main structural motifs, the single-core and the multicore structural motif, were observed for all compound classes. Fragmentation by IRMPD of an isolated mass range was applied for the identification of these molecular building blocks in the organic aerosol extract, revealing the formation of heterocyclic aromatic core structures from the fragmentation of precursor molecules that can be assigned to the multicore structural motif.

Thermal analysis of the peat samples under nitrogen-atmosphere simulating thermal decomposition reactions in smoldering wildfires revealed three mass loss steps in the range of 200–500 °C that are assigned to the degradation of hemicellulose, cellulose, and lignin/humic substances. Simultaneous evolved gas analysis revealed a bimodal distribution in the mass spectrometric data, that are a result of the thermal degradation of hemicellulose and cellulose at lower temperatures, and lignin/humic substances at higher temperatures. Especially the pyrolysis products of the latter revealed interesting insights: In comparison to Arctic peats, the investigated boreal peats are enriched in small single-core pyrolysis products possibly produced by the decomposition of macromolecules like lignin or humic substances. However, as peat is highly variable in its composition, further studies are needed to verify those observations.

The comparison of organic aerosol extracts to the two thermal analysis conditions revealed a higher overlap of shared compounds with TGA under smoldering conditions and a lower overlap for oxidative conditions, which is in good agreement with the observed burning conditions. Furthermore, a similar structural dependency of single-core oxygenated species was observed for all three experimental datasets. Those observations might help to elucidate the formation processes of organic aerosol constituents emitted by the smoldering burning of peat.

The in-depth characterization of the chemical composition of peat burning organic aerosol and its structural motifs as well as their formation in different laboratory-based experiments is an important contribution to increase the understanding of the properties and effects induced by the emissions of real peatland fire emissions. More frequently occurring boreal and Arctic peatland fires can emit PM to the vulnerable Arctic ecosystem, further increasing the climate change in this region due to the potentially strong impact on the snow albedo by the detected structural motifs. Nonetheless, the small-scale laboratory-based approach is limited in simulating the complex organic aerosol formation mechanisms, which points out the need for further research on real combustion facilities and field studies.

### **Supporting information.**

Tables: combustion conditions, intensity weighted sum parameters, compound class number and intensity distribution, thermal analysis mass loss, coordinates of DBE vs. #C regions.

Figures: Upset plot comparison PM extracts, mass spectra with compound class distribution of PM extracts, contour DBE vs. #C plots of PM extracts and IRMPD precursor region, DTG curves, mass loss curve comparison of peat layers, time-resolved survey plots of TGA-FT-ICR MS, mass spectra with compound class distribution of TGA-EGA, compound class distribution of peat TGA-FT-ICR MS, contour DBE vs. #C

plots of TGA-FT-ICR MS, temperature resolved compound class trends, upset plot comparison of TGA and PM extract data.

## **Acknowledgments**

This work was supported by the German Research Foundation (DFG) under grant ZI 764/24-1 and the Research Council of Finland (grant 341597). A portion of the work was performed at the National High Magnetic Field Laboratory ICR User Facility, which is supported by the National Science Foundation Division of Chemistry and Division of Material Research through DMR-1644779 and the State of Florida. H.C. acknowledges funding from the Helmholtz Association (HGF) by the Helmholtz International Laboratory aeroHEALTH (InterLabs-0005). The authors thank the DFG for funding the Bruker FT-ICR MS (INST 264/56). M. M. R. acknowledges support received from Arctic Avenue and the Research Council of Finland projects 355871 and 341271.

## Author Contributions

E. S.: Methodology, Investigation, Formal analysis, Visualization, Writing - Original Draft, Writing - Review & Editing; A. N.: Investigation, Writing - Original Draft, Visualization, Writing - Review & Editing; C. P. R.: Methodology, Software, Resources, Writing - Review & Editing, Supervision, Project administration; M. L. C. P.: Investigation, Recourses, Review & Editing; M. S.: Investigation, Data Curation; M. M. R.: Conceptualization, Investigation, Review & Editing; M. I.: Investigation, Review & Editing; K. K.: Conceptualization, Investigation, Writing - Review & Editing; O. S.: Conceptualization, Investigation, Review & Editing, Supervision, Resources, Funding acquisition; H.C.: Conceptualization, Writing - Review & Editing, Supervision, Project administration; R.Z.: Resources, Writing - Review & Editing, Funding acquisition

## References

- (1) Grant, E.; Runkle, J. D. Long-term health effects of wildfire exposure: A scoping review. *The Journal of Climate Change and Health* **2022**, *6*, 100110.
- (2) Hinwood, A. L.; Rodriguez, C. M. Potential health impacts associated with peat smoke. *Journal of the Royal Society of Western Australia* **2005**, 133–138.
- (3) Turetsky, M. R.; Benscoter, B.; Page, S.; Rein, G.; van der Werf, G. R.; Watts, A. Global vulnerability of peatlands to fire and carbon loss. *Nature Geosci* **2015**, *8* (1), 11–14.
- (4) Lourenco, M.; Woodborne, S.; Fitchett, J. M. Fire regime of peatlands in the Angolan Highlands. *Environ. Monit. Assess.* **2022**, *195* (1), 78.
- (5) Yokelson, R. J.; Saharjo, B. H.; Stockwell, C. E.; Putra, E. I.; Jayarathne, T.; Akbar, A.; Albar, I.; Blake, D. R.; Graham, L. L. B.; Kurniawan, A.; Meinardi, S.; Ningrum, D.; Nurhayati, A. D.; Saad, A.; Sakuntaladewi, N.; Setianto, E.; Simpson, I. J.; Stone, E. A.; Sutikno, S.; Thomas, A.; Ryan, K. C.; Cochrane, M. A. Tropical peat fire emissions: 2019 field measurements in Sumatra and Borneo and synthesis with previous studies. *Atmos. Chem. Phys.* **2022**, *22* (15), 10173–10194.
- (6) Melton, J. R.; Wania, R.; Hodson, E. L.; Poulter, B.; Ringeval, B.; Spahni, R.; Bohn, T.; Avis, C. A.; Beerling, D. J.; Chen, G.; Eliseev, A. V.; Denisov, S. N.; Hopcroft, P. O.; Lettenmaier, D. P.; Riley, W. J.; Singarayer, J. S.; Subin, Z. M.; Tian, H.; Zürcher, S.; Brovkin, V.; van Bodegom, P. M.; Kleinen, T.; Yu, Z. C.; Kaplan, J. O. Present state of global wetland extent and wetland methane modelling: conclusions from a model inter-comparison project (WETCHIMP). *Biogeosciences* **2013**, *10* (2), 753–788.
- (7) Xu, J.; Morris, P. J.; Liu, J.; Holden, J. PEATMAP: Refining estimates of global peatland distribution based on a meta-analysis. *CATENA* **2018**, *160*, 134–140.
- (8) Poulter, B.; Christensen, N. L.; Halpin, P. N. Carbon emissions from a temperate peat fire and its relevance to interannual variability of trace atmospheric greenhouse gases. *J. Geophys. Res.* **2006**, *111* (D6).
- (9) IPCC. *Climate change and land: An IPCC special report on climate change, desertification, land degradation, sustainable land management, food security, and greenhouse gas fluxes in terrestrial ecosystems : summary for policymakers*; Intergovernmental Panel on Climate Change, 2019.

- (10) Descals, A.; Gaveau, D. L. A.; Verger, A.; Sheil, D.; Naito, D.; Peñuelas, J. Unprecedented fire activity above the Arctic Circle linked to rising temperatures. *Science (New York, N.Y.)* **2022**, *378* (6619), 532–537.
- (11) Witze, A. The Arctic is burning like never before - and that's bad news for climate change. *Nature* **2020**, *585* (7825), 336–337.
- (12) Fewster, R. E.; Morris, P. J.; Ivanovic, R. F.; Swindles, G. T.; Peregon, A. M.; Smith, C. J. Imminent loss of climate space for permafrost peatlands in Europe and Western Siberia. *Nat. Clim. Change* **2022**, *12* (4), 373–379.
- (13) Moore, P. D. The ecology of peat-forming processes: a review. *Int. J. Coal Geol.* **1989**, *12* (1-4), 89–103.
- (14) D. W. van Krevelen. Graphical-statistical method for the study of structure and reaction processes of coal. *Fuel* **1950** (29), 269–284.
- (15) Glenn B. Stracher, Anupma Prakash, Guillermo Rein, Ed. *Coal and Peat Fires: a Global Perspective*; Elsevier, 2015.
- (16) Rein, G. Smouldering Fires and Natural Fuels. In *Fire Phenomena and the Earth System*; Belcher, C. M., Ed.; John Wiley & Sons, 2013; pp 15–33. DOI: 10.1002/9781118529539.ch2.
- (17) Yokelson, R. J.; Griffith, D. W. T.; Ward, D. E. Open-path Fourier transform infrared studies of large-scale laboratory biomass fires. *J. Geophys. Res.* **1996**, *101* (D15), 21067–21080.
- (18) Blake, D.; Hinwood, A. L.; Horwitz, P. Peat fires and air quality: volatile organic compounds and particulates. *Chemosphere* **2009**, *76* (3), 419–423.
- (19) Bahureksa, W.; Borch, T.; Young, R. B.; Weisbrod, C. R.; Blakney, G. T.; McKenna, A. M. Improved Dynamic Range, Resolving Power, and Sensitivity Achievable with FT-ICR Mass Spectrometry at 21 T Reveals the Hidden Complexity of Natural Organic Matter. *Anal. Chem.* **2022**, *94* (32), 11382–11389.
- (20) Williams, M. L.; Olomukoro, A. A.; Emmons, R. V.; Godage, N. H.; Gionfriddo, E. Matrix effects demystified: Strategies for resolving challenges in analytical separations of complex samples. *J. Sep. Sci.* **2023**, *46* (23), e2300571.
- (21) Schneider, E.; Rüger, C. P.; Chacón-Patiño, M. L.; Somero, M.; Ruppel, M. M.; Ihalainen, M.; Köster, K.; Sippula, O.; Czech, H.; Zimmermann, R. The complex composition of organic aerosols emitted during burning varies between Arctic and boreal peat. *Commun. Earth Environ.* **2024**, *5* (1).
- (22) Hugelius, G.; Loisel, J.; Chadburn, S.; Jackson, R. B.; Jones, M.; MacDonald, G.; Marushchak, M.; Olefeldt, D.; Packalen, M.; Siewert, M. B.; Treat, C.; Turetsky, M.; Voigt, C.; Yu, Z. Large stocks of peatland carbon and nitrogen are vulnerable to permafrost thaw. *PNAS* **2020**, *117* (34), 20438–20446.
- (23) Hu, Y.; Fernandez-Anez, N.; Smith, T. E. L.; Rein, G. Review of emissions from smouldering peat fires and their contribution to regional haze episodes. *Int. J. Wildland Fire* **2018**, *27* (5), 293.
- (24) Chen, H.; Zhao, W.; Liu, N. Thermal Analysis and Decomposition Kinetics of Chinese Forest Peat under Nitrogen and Air Atmospheres. *Energy Fuels* **2011**, *25* (2), 797–803.
- (25) Yang, J.; Chen, H.; Zhao, W.; Zhou, J. TG-FTIR-MS study of pyrolysis products evolving from peat. *J. Anal. Appl. Pyrolysis* **2016**, *117*, 296–309.
- (26) Friederici, L.; Meščeriakovė, S.-M.; Neumann, A.; Sermyagina, E.; Meščeriakovas, A.; Lähde, A.; Grimmer, C.; Streibel, T.; Rüger, C. P.; Zimmermann, R. Effect of hydrothermal carbonization and eutectic salt mixture (KCl/LiCl) on the pyrolysis of Kraft lignin as revealed by thermal analysis coupled to advanced high-resolution mass spectrometry. *J. Anal. Appl. Pyrolysis* **2022**, *166*, 105604.
- (27) Samburova, V.; Schneider, E.; Rüger, C. P.; Inouye, S.; Sion, B.; Axelrod, K.; Bahdanovich, P.; Friederici, L.; Raeofy, Y.; Berli, M.; Lutz, A.; Zimmermann, R.; Moosmüller, H. Modification of Soil

Hydroscopic and Chemical Properties Caused by Four Recent California, USA Megafires. *Fire* **2023**, *6* (5), 186.

(28) Neumann, A.; Chacón-Patiño, M. L.; Rodgers, R. P.; Rüger, C. P.; Zimmermann, R. Investigation of Island/Single-Core- and Archipelago/Multicore-Enriched Asphaltenes and Their Solubility Fractions by Thermal Analysis Coupled with High-Resolution Fourier Transform Ion Cyclotron Resonance Mass Spectrometry. *Energy Fuels* **2021**, *35* (5), 3808–3824.

(29) Chacón-Patiño, M. L.; Rowland, S. M.; Rodgers, R. P. Advances in Asphaltene Petroleomics. Part 1: Asphaltenes Are Composed of Abundant Island and Archipelago Structural Motifs. *Energy Fuels* **2017**, *31* (12), 13509–13518.

(30) Chacón-Patiño, M. L.; Gray, M. R.; Rüger, C.; Smith, D. F.; Glattke, T. J.; Niles, S. F.; Neumann, A.; Weisbrod, C. R.; Yen, A.; McKenna, A. M.; Giusti, P.; Bouyssiere, B.; Barrère-Mangote, C.; Yarranton, H.; Hendrickson, C. L.; Marshall, A. G.; Rodgers, R. P. Lessons Learned from a Decade-Long Assessment of Asphaltenes by Ultrahigh-Resolution Mass Spectrometry and Implications for Complex Mixture Analysis. *Energy Fuels* **2021**, *35* (20), 16335–16376.

(31) Martens, P.; Czech, H.; Orasche, J.; Abbaszade, G.; Sklorz, M.; Michalke, B.; Tissari, J.; Bizjak, T.; Ihalainen, M.; Suhonen, H.; Yli-Pirilä, P.; Jokiniemi, J.; Sippula, O.; Zimmermann, R. Brown Coal and Logwood Combustion in a Modern Heating Appliance: The Impact of Combustion Quality and Fuel on Organic Aerosol Composition. *Environ. Sci. Technol.* **2023**, *57* (14), 5532–5543.

(32) Richter, H.; Howard, J. Formation of polycyclic aromatic hydrocarbons and their growth to soot—a review of chemical reaction pathways. *Prog. Energy Combust. Sci.* **2000**, *26* (4-6), 565–608.

(33) DiDonato, N.; Chen, H.; Waggoner, D.; Hatcher, P. G. Potential origin and formation for molecular components of humic acids in soils. *Geochim. Cosmochim. Acta* **2016**, *178*, 210–222.

(34) Vasilevich, R.; Lodygin, E.; Beznosikov, V.; Abakumov, E. Molecular composition of raw peat and humic substances from permafrost peat soils of European Northeast Russia as climate change markers. *The Science of the total environment* **2018**, *615*, 1229–1238.

(35) University of Eastern Finland. *ILMARI - Aerosol physics, chemistry and toxicology research unit*. [www.uef.fi/ilmari](http://www.uef.fi/ilmari) (accessed 2024-03-13).

(36) Rüger, C. P.; Sklorz, M.; Schwemer, T.; Zimmermann, R. Characterisation of ship diesel primary particulate matter at the molecular level by means of ultra-high-resolution mass spectrometry coupled to laser desorption ionisation—comparison of feed fuel, filter extracts and direct particle measurements. *Anal. Bioanal. Chem.* **2015**, *407* (20), 5923–5937.

(37) Friederici, L.; Schneider, E.; Burnens, G.; Streibel, T.; Giusti, P.; Rüger, C. P.; Zimmermann, R. Comprehensive Chemical Description of Pyrolysis Chars from Low-Density Polyethylene by Thermal Analysis Hyphenated to Different Mass Spectrometric Approaches. *Energy Fuels* **2021**, *35* (22), 18185–18193.

(38) Rüger, C. P.; Miersch, T.; Schwemer, T.; Sklorz, M.; Zimmermann, R. Hyphenation of Thermal Analysis to Ultrahigh-Resolution Mass Spectrometry (Fourier Transform Ion Cyclotron Resonance Mass Spectrometry) Using Atmospheric Pressure Chemical Ionization For Studying Composition and Thermal Degradation of Complex Materials. *Anal. Chem.* **2015**, *87* (13), 6493–6499.

(39) Hendrickson, C. L.; Quinn, J. P.; Kaiser, N. K.; Smith, D. F.; Blakney, G. T.; Chen, T.; Marshall, A. G.; Weisbrod, C. R.; Beu, S. C. 21 Tesla Fourier Transform Ion Cyclotron Resonance Mass Spectrometer: A National Resource for Ultrahigh Resolution Mass Analysis. *J. Am. Soc. Mass Spectrom.* **2015**, *26* (9), 1626–1632.

(40) Rüger, C. P.; Schwemer, T.; Sklorz, M.; O'Connor, P. B.; Barrow, M. P.; Zimmermann, R. Comprehensive chemical comparison of fuel composition and aerosol particles emitted from a ship

diesel engine by gas chromatography atmospheric pressure chemical ionisation ultra-high resolution mass spectrometry with improved data processing routines. *European journal of mass spectrometry (Chichester, England)* **2017**, *23* (1), 28–39.

(41) Eric Schneider; Dr Martha Liliana Chacon-Patino. *Low-polar peat burning organic aerosol: composition, structural motifs and formation:[data repository]*.

(42) Cho, Y.; Kim, Y. H.; Kim, S. Planar limit-assisted structural interpretation of saturates/aromatics/resins/asphaltenes fractionated crude oil compounds observed by Fourier transform ion cyclotron resonance mass spectrometry. *Anal. Chem.* **2011**, *83* (15), 6068–6073.

(43) Lobodin, V. V.; Marshall, A. G.; Hsu, C. S. Compositional space boundaries for organic compounds. *Anal. Chem.* **2012**, *84* (7), 3410–3416.

(44) Barneto, A. G.; Carmona, J. A.; Alfonso, J. E. M.; Ferrer, J. A. C. Use of Thermogravimetry/Mass Spectrometry Analysis to Explain the Origin of Volatiles Produced during Biomass Pyrolysis. *Ind. Eng. Chem. Res.* **2009**, *48* (15), 7430–7436.

(45) Yatavelli, R. L. N.; Chen, L.-W. A.; Knue, J.; Samburova, V.; Gyawali, M.; Watts, A. C.; Chakrabarty, R. K.; Moosmüller, H.; Hodzic, A.; Wang, X.; Zielinska, B.; Chow, J. C.; Watson, J. G. Emissions and Partitioning of Intermediate-Volatility and Semi-Volatile Polar Organic Compounds (I/SV-POCs) During Laboratory Combustion of Boreal and Sub-Tropical Peat. *Aerosol Sci Eng* **2017**, *1* (1), 25–32.

(46) Czech, H.; Miersch, T.; Orasche, J.; Abbaszade, G.; Sippula, O.; Tissari, J.; Michalke, B.; Schnelle-Kreis, J.; Streibel, T.; Jokiniemi, J.; Zimmermann, R. Chemical composition and speciation of particulate organic matter from modern residential small-scale wood combustion appliances. *The Science of the total environment* **2018**, *612*, 636–648.

(47) Iinuma, Y.; Brüggemann, E.; Gnauk, T.; Müller, K.; Andreae, M. O.; Helas, G.; Parmar, R.; Herrmann, H. Source characterization of biomass burning particles: The combustion of selected European conifers, African hardwood, savanna grass, and German and Indonesian peat. *J. Geophys. Res.* **2007**, *112* (D8).

(48) Lin, C.; Ceburnis, D.; Hellebust, S.; Buckley, P.; Wenger, J.; Canonaco, F.; Prévôt, A. S. H.; Huang, R.-J.; O'Dowd, C.; Ovadnevaite, J. Characterization of Primary Organic Aerosol from Domestic Wood, Peat, and Coal Burning in Ireland. *Environmental science & technology* **2017**, *51* (18), 10624–10632.

(49) Mitra, T.; Zhang, T.; Sediako, A. D.; Thomson, M. J. Understanding the formation and growth of polycyclic aromatic hydrocarbons (PAHs) and young soot from n-dodecane in a sooting laminar coflow diffusion flame. *Combust. Flame* **2019**, *202*, 33–42.

(50) Ye, Y.; Zhan, H.; Yu, X.; Li, J.; Wang, X.; Xie, Z. Detection of organosulfates and nitrooxy-organosulfates in Arctic and Antarctic atmospheric aerosols, using ultra-high resolution FT-ICR mass spectrometry. *The Science of the total environment* **2021**, *767*, 144339.

(51) Purcell, J. M.; Juyal, P.; Kim, D.-G.; Rodgers, R. P.; Hendrickson, C. L.; Marshall, A. G. Sulfur Speciation in Petroleum: Atmospheric Pressure Photoionization or Chemical Derivatization and Electrospray Ionization Fourier Transform Ion Cyclotron Resonance Mass Spectrometry. *Energy Fuels* **2007**, *21* (5), 2869–2874.

(52) Kosyakov, D. S.; Ul'yanovskii, N. V.; Latkin, T. B.; Pokryshkin, S. A.; Berzhonskis, V. R.; Polyakova, O. V.; Lebedev, A. T. Peat burning - An important source of pyridines in the earth atmosphere. *Environmental pollution (Barking, Essex : 1987)* **2020**, *266* (Pt 1), 115109.

(53) Ehrmann, B. M.; Henriksen, T.; Cech, N. B. Relative importance of basicity in the gas phase and in solution for determining selectivity in electrospray ionization mass spectrometry. *Journal of the American Society for Mass Spectrometry* **2008**, *19* (5), 719–728.

(54) Neumann, A.; Tiemann, O.; Hansen, H. J.; Rügner, C. P.; Zimmermann, R. Detailed Comparison of Xenon APPI (9.6/8.4 eV), Krypton APPI (10.6/10.0 eV), APCI, and APLI (266 nm) for Gas Chromatography

High Resolution Mass Spectrometry of Standards and Complex Mixtures. *J. Am. Soc. Mass Spectrom.* **2023**, *34* (8), 1632–1646.

(55) Chacón-Patiño, M. L.; Rowland, S. M.; Rodgers, R. P. Advances in Asphaltene Petroleomics. Part 2: Selective Separation Method That Reveals Fractions Enriched in Island and Archipelago Structural Motifs by Mass Spectrometry. *Energy Fuels* **2018**, *32* (1), 314–328.

(56) Sleno, L.; Volmer, D. A. Ion activation methods for tandem mass spectrometry. *J. Mass Spectrom.* **2004**, *39* (10), 1091–1112.

(57) Dong, C.; Hu, W.; Wang, Y.; Zhang, Y.; Zhu, G.; Han, Y. Double-bond equivalence linear equations for structural interpretation of fossil hydrocarbons. *Fuel* **2023**, *332*, 126206.

(58) Rein, G.; Cleaver, N.; Ashton, C.; Pironi, P.; Torero, J. L. The severity of smouldering peat fires and damage to the forest soil. *CATENA* **2008**, *74* (3), 304–309.

(59) Zhang, Y.; Metz, J. N.; Gross, A. S.; Siskin, M. Unexpected Structural Effects on the Onset of Thermal Reactions of Aromatic Hydrocarbons. *Energy Fuels* **2023**, *37* (8), 5792–5804.

(60) Juselius, T.; Ravolainen, V.; Zhang, H.; Piilo, S.; Müller, M.; Gallego-Sala, A.; Väiliranta, M. Newly initiated carbon stock, organic soil accumulation patterns and main driving factors in the High Arctic Svalbard, Norway. *Scientific reports* **2022**, *12* (1), 4679.

(61) Kovaleva, N. O.; Kovalev, I. V. Transformation of lignin in surface and buried soils of mountainous landscapes. *Eurasian Soil Sci.* **2009**, *42* (11), 1270–1281.

(62) Sutradhar, S.; Fatehi, P. Latest development in the fabrication and use of lignin-derived humic acid. *Biotechnol. Biofuels Bioprod.* **2023**, *16* (1), 38.

(63) Waksman, S. A. *Humus: Origin, chemical composition and importance in nature*, 1936.

(64) Yang, H.; Yan, R.; Chen, H.; Lee, D. H.; Zheng, C. Characteristics of hemicellulose, cellulose and lignin pyrolysis. *Fuel* **2007**, *86* (12–13), 1781–1788.

(65) Mase, C.; Hubert-Roux, M.; Afonso, C.; Giusti, P. Contribution of atmospheric pressure chemical ionization mass spectrometry for the characterization of bio-oils from lignocellulosic biomass: Comparison with electrospray ionization and atmospheric pressure photoionization. *Journal of Analytical and Applied Pyrolysis* **2022**, *167*, 105694.

(66) Laskin, A.; Smith, J. S.; Laskin, J. Molecular characterization of nitrogen-containing organic compounds in biomass burning aerosols using high-resolution mass spectrometry. *Environ. Sci. Technol.* **2009**, *43* (10), 3764–3771.

(67) Benedict, K. B.; Prenni, A. J.; Carrico, C. M.; Sullivan, A. P.; Schichtel, B. A.; Collett, J. L. Enhanced concentrations of reactive nitrogen species in wildfire smoke. *Atmos. Environ.* **2017**, *148*, 8–15.

(68) Serebrennikova, O. V.; Russkikh, I. V.; Strel'nikova, E. B.; Kharanzhevskaya, Y. A.; Fedorov, D. V. Composition of the Organic Compounds of Different Peat Types from the Southern Taiga Subzone of Western Siberia. *Solid Fuel Chem.* **2023**, *57* (1), 21–28.

(69) He, D.; Huang, H.; Arismendi, G. G. n-Alkane distribution in ombrotrophic peatlands from the northeastern Alberta, Canada, and its paleoclimatic implications. *Palaeogeography, Palaeoclimatology, Palaeoecology* **2019**, *528*, 247–257.

(70) Solihat, N. N.; Yustiawati; Kim, S.; Kim, S. Elucidating molecular level impact of peat fire on soil organic matter by laser desorption ionization Fourier transform ion cyclotron resonance mass spectrometry. *Anal. Bioanal. Chem.* **2019**, *411* (27), 7303–7313.

**For Table of Content (TOC) Only**

